Air release measurements of V-oil 1404 downstream of a micro orifice at choked flow conditions

H-A Freudigmann[1], U Iben[1], P F Pelz[2]

[1]Robert Bosch GmbH, Robert-Bosch-Campus 1, D-71272 Renningen, Germany
[2]Chair of Fluid Systems, TU Darmstadt, D-64289 Darmstadt, Germany

E-mail: hans-arndt.freudigmann@de.bosch.com, uwe.iben@de.bosch.com, peter.pelz@fst.tu-darmstadt.de

Abstract. This study presents measurements on air release of V-oil 1404 in the back flow of a micro orifice at choked flow conditions using a shadowgraph imaging method. The released air was determined at three positions downstream of the orifice for different pressure conditions. It was found that more than 23 % of the initially dissolved air is released and appears downstream of the orifice in the form of bubbles.

1. Introduction

Dissolved air in hydraulic liquids often compromises the functionality of hydraulic systems as the air can be released in form of small bubbles. The resulting two phase system has an increased compressibility and a decreased density and viscosity. In hydraulic systems this can lead to reduced system stiffness, vibrations, noise, fluctuation of the mass flow rate and aging of the liquid due to oxidation and generation of carbon residues caused by micro-diesel effects [1–3]. As typical mineral-oil based hydraulic liquids can dissolve a high amount of air (7 -12 Vol.-%, [1, 4]), degassing caused by lowering the static pressure of the liquid below the saturation pressure can lead to a considerable amount of free air. Degassing due to pressure reduction can therefore occur in the suction section of pumps [5], in hydraulic resistances such as valves or throttles [6] or in volume elements such as pipelines during pressure transients [7]. Moreover, experiments [4, 8] and theoretical considerations [9] demonstrate that hydrodynamic cavitation significantly affects the degassing dynamics of liquids. This has to be considered during the design process for robust hydraulic systems using appropriate models. In order to develop and validate these models experimental data are required.

To the authors knowledge and beside the previously mentioned work, this is the first systematic study investigating quantitatively the linkage of hydrodynamic cavitation and air release. In this work close attention is paid to the bubbly flow downstream of a cylindrical orifice at choked flow conditions. The flow is investigated in a channel of rectangular cross section applying a shadowgraph imaging method at three positions. The recorded images were processed using a developed bubble segmentation algorithm.

2. Materials and Methods

Shell V-oil 1404 (ISO 4113) is widely used as a testing oil for diesel injection systems and its liquid properties are well-known [10, 11]. Figure 1a) illustrates the experimental setup. A stirrer

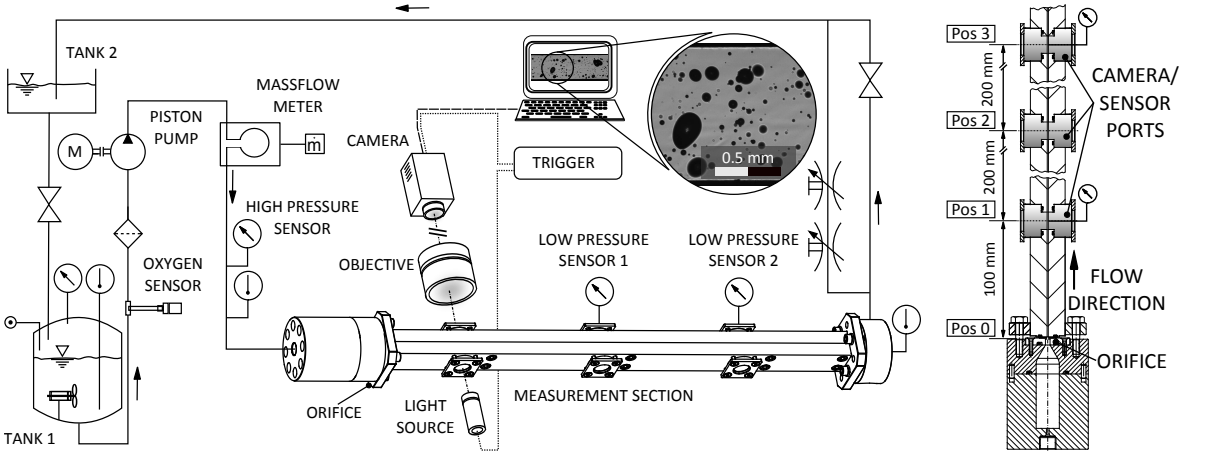

(a) Test rig scheme. **(b)** Measurement section.

Figure 1: Schematics of the experimental setup.

in the supply tank "TANK 1" ensures that the liquid is homogeneously saturated with air at atmospheric pressure conditions. During the experiment the gas volume above the liquid in "TANK 1" is increased by about 0.4 bar above atmospheric pressure to avoid degassing in the suction line of the speed-variable piston pump. Due to the long time-scales for the diffusion process, the increased gas pressure has virtually no influence on the initial concentration of the dissolved gas. An oxygen sensor (Hamilton, VisiFerm DO Arc 120) upstream of the pump is used for measuring the partial oxygen pressure allowing for monitor the saturation of the liquid with air. Rearward of the piston pump a mass flow meter (Siemens F C MASS 2100 DI 1.5), a high pressure sensor (Kistler 4065, 200 bar) and a temperature sensor are installed. The temperature of the liquid in "TANK 1" is between 23 °C and 25 °C.

Figure 1b) illustrates the measurement section in detail. The liquid passes a cylindrical micro orifice with 0.2 mm in diameter and 2 mm in length at "Pos 0". Rearward of the orifice the flow is released into a square flow channel with 1 mm × 1 mm in size. In this channel three ports are installed where the pressure is measured at two positions (Althen XPC10 35 bar) and the flow is observed with a camera at a third position. The positions of the pressure sensors and the camera are interchangeable. Two throttling valves are placed in series downstream of the square flow channel which enable an adjustment of the outlet pressure rearward of the orifice. Liquid which has passed the measurement section is collected in "TANK 2". Sensor signals are gathered by NI DAQ data acquisition cards (National Instruments) with a sampling rate of 1 kHz.

For observing the flow in the channel a shadowgraph technique is used with a spark flash (Impulsphysik GmbH, Nanolite EGG FX 800) as a light source, an objective (B. Halle, f=100 mm, k=2) and a camera (PCO 2000) similar to the setup described in [4]. The camera and the flash are synchronized; the applied exposure rate is 2 Hz with an exposure time of 1 µs of the camera. The scaling factor of the optical setup is 1.6 µm per pixel with a magnification of 4.6. For each operation point 100 images were evaluated.

Depending on the operation conditions, bubbles can be observed in the flow downstream of the orifice, cf. Figure 1a). In order to analyze the bubbles in the obtained shadowgraph images a segmentation algorithm was developed. The algorithm detects spherical bubbles using the Hough-Transformation and non-spherical bubbles using a histogram based binarization, cf. Figure 2a). The radii of the spherical bubbles are determined at the half irradiance level of the intensity profiles [12]. The radii of spherical out-of-focus bubbles are corrected using an empirical correction function applying the contrast of the bubble leading to sizing errors less

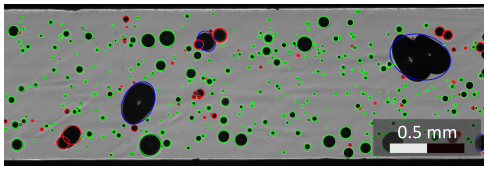

(a) Result of the bubble recognition.

(b) Cavitation plume.

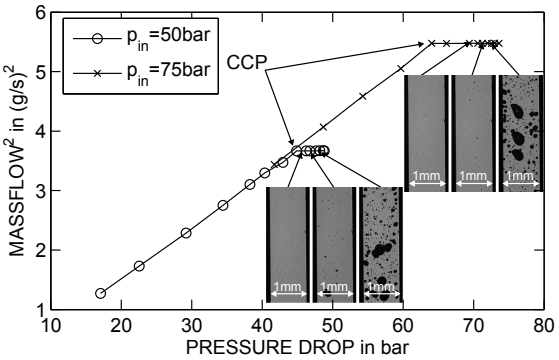

(c) Mass flow behavior of the cylindrical orifice.

Figure 2: a) Green circles indicate bubbles with an evaluated intensity profile. Due to overlaps, this was not possible for the red marked bubbles. Blue lines illustrate the best fitting ellipses for non-spherical bubbles. b) Exemplary image of the cavitation plume representing the average of 100 shadowgraph images at "Pos 0" recorded in a transparent channel located directly at the orifice exit. c) Mass flow behavior of the orifice and exemplary images of the bubbley flow for two fixed inlet pressures p_{in}. The outlet pressure was measured 101 mm downstream of the orifice.

than 10 %. The volume of a non-spherical bubble is approximated as two spheroids based on the best fitting ellipse. Errors due to mutually concealing bubbles were not taken into account. The detection algorithm was validated with manually evaluated bubble images.

3. Results

As the present study focuses on the appearance of bubbles in the backflow of an orifice at choked flow conditions, the mass flow characteristic of the used orifice is presented in Figure 2c). It is obtained using a pressure resistant flow channel with a cross-section area identical to the channel shown in Figure 1b). As expected, the square of the mass flow rate is proportional to the pressure drop over the orifice for operating points with no cavitation occurring. For a critical value of the pressure drop (Critical Cavitation Point CCP) significant cavitation occurs, cf. Figure 2b) and the mass flow is independent of the outlet pressure. For the region beyond the CCP bubbles can be observed in the backflow of the orifice e.g. at "Pos 1" as shown in Figure 2c). Images of the bubbly flow were recorded at three positions ("Pos 1"-"Pos 3") for two fixed inlet pressures, several outlet pressures and constant mass flow rates due to choked flow conditions. The observed bubbles downstream of the orifice tend to be spherical for smaller bubbles and non-spherical for larger bubbles. Bubble diameters range from around 7 µm up to 0.5 mm (spherical equivalent diameter). The bubbles are assumed to be completely filled with air due to the high liquid pressure in the channel (>1.3 bar) compared to the vapor pressure of the liquid (<10 Pa, [11]).

The mass fraction of the initially dissolved air c_g in the suction line of the piston pump is determined by measuring the partial pressure of oxygen in the liquid, cf. Figure 1a). The ratio of the partial pressures of oxygen to air in the liquid is assumed to equal the ratio of the partial pressures of oxygen to air in the atmosphere. Hence, the pressure of dissolved air in the liquid can be determined. Knowing the Ostwald-Coefficient of the liquid for air (L_V=12 Vol.-% at 25 °C, [4]) the concentration of initially dissolved air (0.169 mass-‰± 1 %) is determined by employing Henry's law. To determine the amount of gas contained by the bubbles according to [4] the obtained images are analyzed using the presented bubble segmentation algorithm. Figures 3a) and 3b) show the mass fraction of the degassed air $\xi := \frac{m_g}{m_l \cdot c_g} \cdot 100\%$ for the stated conditions at three distances downstream of the orifice. ξ is defined as the ratio of the degassed air mass m_g to the initially dissolved air mass m_l in a liquid element.

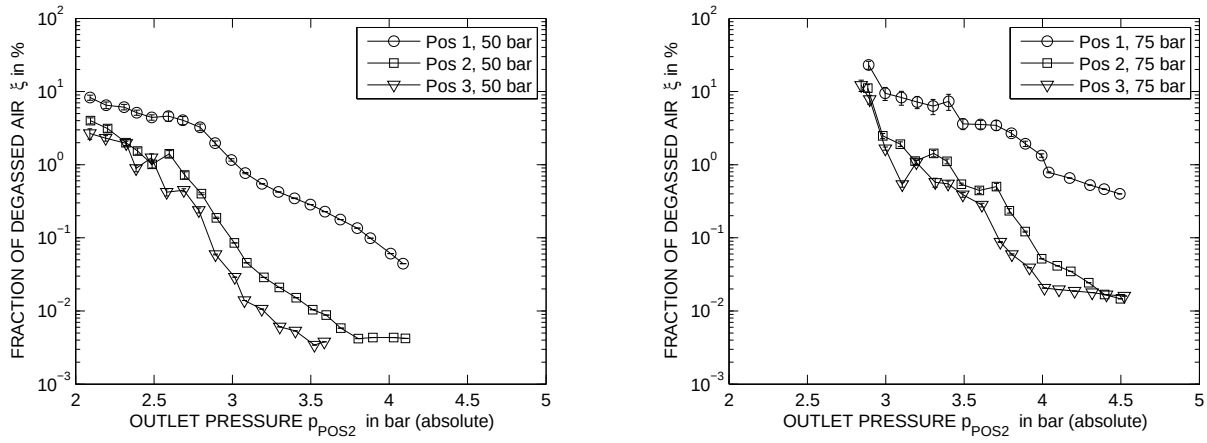

(a) $p_{in} = 50\,\mathrm{bar}$ **(b)** $p_{in} = 75\,\mathrm{bar}$

Figure 3: Mass fraction of released air ξ for two fixed inlet pressures and several outlet pressures. Non-spherical bubbles are treated as spheroids by rotating the best fitting ellipsis of the shadowgraph image about its major or minor axis. The differences in the bubble volumes for each rotating axis are indicated by the error bars.

According to the results for a different orifice presented by Iben et al. [4] the release of air at choked flow conditions is very sensitive to the outlet pressure showing a nearly exponential relationship. The measurements at different positions for similar operating points show that the amount of free air is less at "Pos 2" than at "Pos 1". This is due to the reabsorption of the released air in the undersaturated liquid. However, the differences between "Pos 2" and "Pos 3" in the amount of free air are less significant.

4. Conclusion

The presented results show how hydrodynamic cavitation in an orifice is associated with a substantial increase of free air downstream of a cavitating regime. In addition the results reveal that a significant amount of the released air is reabsorbed into the liquid while traveling downstream and therefore extend the findings of Iben et al. The results can serve as validation data for modeling approaches of air release phenomena in hydraulics.

References

[1] Bock W, Braun J, Puhl N and Heinemann H 2010 Air release properties of hydraulic fluids *IFK, Internationals Fluidtechnisches Kolloquium* vol 7 pp 327–340
[2] Ruan J and Burton R 2006 Bulk modulus of air content oil in a hydraulic cylinder *ASME 2006 International Mechanical Engineering Congress and Exposition* (American Society of Mechanical Engineers) pp 259–269
[3] Backé W and Lipphardt P 1976 *CI Mech. Eng. C97/76*
[4] Iben U, Wolf F, Freudigmann H A, Fröhlich J and Heller W 2015 *Experiments in Fluids* **56** 1–10
[5] Zhou J, Vacca A and Casoli P 2014 *Simulation Modelling Practice and Theory* **45** 35–49
[6] Lichtarowicz A and Pearce I D 1974 Cavitation and aeration effects in long orifices *Cavitation Conference, Institution Mechanical Engineers, Edinburgh* vol 19 p 74
[7] Wiggert D and Sundquist M 1979 *Journal of Fluids Engineering* **101** 79–86
[8] Sato K, Liu Z and Brennen C 1993 The micro-bubble distribution in the wake of a cavitating circular cylinder *ASME* 153 (American Society of Mechanical Engineers) pp 75–80
[9] Watanabe M and Prosparetti A 1994 The effect of gas diffusion on the nuclei population downstream of a cavitation zone vol 190 (ASME) pp 211–211
[10] Ndiaye E H I, Bazile J P, Nasri D, Boned C and Daridon J L 2012 *Fuel* **98** 288–294
[11] Chorążewski M, Dergal F, Sawaya T, Mokbel I, Grolier J P E and Jose J 2013 *Fuel* **105** 440–450
[12] Bongiovanni C, Chevaillier J P and Fabre J 1997 *Experiments in Fluids* **23** 209–216